



HAL
open science

A Time-Domain Perspective on the Structural and Electronic Response in Epitaxial Ferroelectric Thin Films on Silicon

Christelle Kwamen, Matthias Rössle, Wolfram Leitenberger, Pedro Rojo Romeo, Bertrand Vilquin, Catherine Dubourdieu, Matias Bargheer

► **To cite this version:**

Christelle Kwamen, Matthias Rössle, Wolfram Leitenberger, Pedro Rojo Romeo, Bertrand Vilquin, et al.. A Time-Domain Perspective on the Structural and Electronic Response in Epitaxial Ferroelectric Thin Films on Silicon. *Nano Letters*, 2024, 10.1021/acs.nanolett.4c00712 . hal-04660491

HAL Id: hal-04660491

<https://hal.science/hal-04660491>

Submitted on 26 Jul 2024

HAL is a multi-disciplinary open access archive for the deposit and dissemination of scientific research documents, whether they are published or not. The documents may come from teaching and research institutions in France or abroad, or from public or private research centers.

L'archive ouverte pluridisciplinaire **HAL**, est destinée au dépôt et à la diffusion de documents scientifiques de niveau recherche, publiés ou non, émanant des établissements d'enseignement et de recherche français ou étrangers, des laboratoires publics ou privés.

A time-domain perspective on the structural and electronic response in epitaxial ferroelectric thin films on silicon

C. Kwamen,¹ M. Rössle,¹ W. Leitenberger,² P. Rojo Romeo,³ B. Vilquin,³ C. Dubourdieu*,^{4,5, a)} and M. Bargheer*^{2, 1, b)}

¹⁾ Helmholtz-Zentrum Berlin für Materialien und Energie, Wilhelm-Conrad-Röntgen Campus, BESSY II, Albert-Einstein-Str. 15, 12489 Berlin, Germany

²⁾ Institut für Physik & Astronomie, Universität Potsdam, Karl-Liebknecht-Str. 24-25, 14476 Potsdam, Germany

³⁾ Univ. Lyon, Institut des Nanotechnologies de Lyon (UMR5270/CNRS), Ecole Centrale de Lyon, 36 avenue Guy de Collongue, 69134, Ecully Cedex, France

⁴⁾ Helmholtz-Zentrum Berlin für Materialien und Energie, Institute Functional Oxides for Energy Efficient Information Technology (IFOX), Hahn-Meitner-Platz 1, 14109 Berlin, Germany

⁵⁾ Freie Universität Berlin, Physical and Theoretical Chemistry, Arnimallee 22, 14195 Berlin, Germany

(Dated: May 27, 2024)

Abstract This *operando* study of the structural response of epitaxial ferroelectric $\text{Pb}(\text{Zr}_{0.48}\text{Ti}_{0.52})\text{O}_3$ capacitors grown on Silicon substrates reports synchrotron radiation based diffraction experiments during hysteresis loop measurements in the kHz frequency range. We explain the rounding of the polarization ($P-U$) and strain ($\eta-U$) hysteresis loops in a time-domain perspective: The polarization and the structural motion within the unit cell are coupled to the strain along the c -axis by the piezoelectric effect. The driving stress $\sigma(t)$ is calculated as the product of the voltage $U(t)$ and polarization $P(t)$, which lags behind $U(t)$ when the domain wall velocity is too slow to support high frequencies. Unlike electrical variables, the driving stress and the lattice strain $\eta(t)$ oscillate at twice the frequency of the applied electrical field. We extract the phase shift $\phi_{\sigma-\eta}$ of the strain to the driving stress due to damping of the structural motion.

Ferroelectric (FE) thin films are technologically important and are found in different applications in our daily lives. For example, FEs are used for non-volatile memories because of the ability to switch their polarization under an applied electric field or for sensor and actuator devices exploiting the strong coupling of electric field E and mechanical strain η ¹⁻³. These physical properties scale with the device size and are strongly frequency-dependent⁴⁻⁶. From an application standpoint, there is a growing interest in using ferroelectrics monolithically integrated on silicon since this is the CMOS-based technology platform. In the past 15 years, many efforts have been devoted to the epitaxial growth of various perovskite ferroelectrics such as BaTiO_3 , PbTiO_3 or $\text{Pb}(\text{Zr}_{1-x}\text{Ti}_x)\text{O}_3$ on silicon or GaAs ⁷⁻¹². The ferroelectric lead-based solid solution $\text{Pb}(\text{Zr}_{1-x}\text{Ti}_x)\text{O}_3$ is of particular interest due to its large piezoelectric coefficients¹³. Enhanced piezoelectric properties are observed at the morphotropic phase boundary in the composition range $0.47 < x \leq 0.52$ that separates a Ti-rich tetragonal from a Zr-rich rhombohedral phase by a monoclinic intermediate phase¹⁴⁻¹⁸. Few groups have reported the integration of epitaxial lead titanate films into capacitors on silicon substrates^{10,18-21}. Advantages of epitaxial films over polycrystalline ones include a well-defined polar axis and a smaller thickness (for achieving the

same remanent polarization) and thus requiring a lower voltage for polarization switching. For device applications, a key feature is the dynamics of the polarization switching and of the coupled electromechanical response. In FE devices, the dynamical response spans the wide time range from sub-ps time scales^{22,23} over ns for domain dynamics²⁴⁻²⁹. The switching dynamics in epitaxial films has been widely studied in micrometer scale capacitors and is well described by the Kolmogorov-Avrami-Ishibashi (KAI) model³⁰⁻³³. In this model, the switching kinetics is governed by the dynamics of domain nucleation, growth, and coalescence assuming nucleation of domains at independent nucleation centers. For FE thin films, *in-situ* synchrotron X-ray diffraction has become available to quantify the electromechanical response and fatigue³⁴⁻³⁶. Few experiments are reported on single-crystalline films with the c -axis oriented perpendicular to the substrate surface^{14,24,37,38}. The simultaneous characterization of strain and polarization reported for ceramics³⁹ was extended to thin films^{27,28,40}. However, to the best of our knowledge, time-resolved studies of the coupled dynamics of polarization and strain in ferroelectrics integrated on silicon and systematic experimental studies on the frequency-dependence structural response have not yet been reported.

In this paper we report an *operando* study of the electro-mechanical coupling and its dynamics determined by simultaneous synchrotron X-ray diffraction and hysteresis-loop measurements at various frequencies of a thin epitaxial ferroelectric $\text{Pb}(\text{Zr}_{0.48}\text{Ti}_{0.52})\text{O}_3$ (PZT) film deposited on (001) Si and sandwiched between two metal-

^{a)} Electronic mail: catherine.dubourdieu@helmholtz-berlin.de

^{b)} Electronic mail: bargheer@uni-potsdam.de

lic electrodes. The PZT film composition was chosen within the morphotropic phase boundary. We measure the time-dependence of the ferroelectric polarization $P(t)$ and of the lattice strain $\eta(t)$ of the PZT film for frequencies varying from 2 up to 200 kHz. We discuss the complex phenomenon of the periodically driven modulation of the ferroelectric polarization coupled to the structural deformation in terms of a oscillator equations, which describe the dielectric displacement and the motion of the atoms within the unit cell along the FE soft mode⁴¹. We find that the piezoelectric driving stress $\sigma(t) \propto U(t)P(t)$ oscillates at twice the frequency of the driving voltage $U(t)$. We show that the phase delay $\phi_{\sigma-\eta}$ between the stress and the strain increases with the driving frequency and we demonstrate that this phase lag **contributes to the rounding of the structural $\eta-U$ and electrical $P-U$ hysteresis loops of the FE at high frequencies.**

A 200 nm thick epitaxial (001) oriented $\text{Pb}(\text{Zr}_{0.48}\text{Ti}_{0.52})\text{O}_3$ (PZT) film with a chemical composition reflecting that of the MPB of the Pb-Zr-Ti-O phase diagram was deposited by RF magnetron sputtering onto a sputtered 30 nm thick epitaxial SrRuO_3 (SRO) bottom electrode on a SrTiO_3 epitaxial seed layer grown by molecular beam epitaxy on a (001) Si substrate. The details of all deposition processes can be found in⁴²⁻⁴⁵. After the PZT deposition, in order to crystallize the FE film, the sample was flash-annealed at 650°C for one minute under oxygen atmosphere. Circular Pt top electrodes with radii between 50 and 300 μm were then deposited by sputtering and structured using a UV photolithography lift-off process⁴⁶.

The time-resolved ultrafast X-ray diffraction measurements under applied electrical field were performed at the KMC-3 XPP⁴⁷ endstation of the storage ring BESSY II, Berlin, Germany, operated in hybrid mode⁴⁸. The results presented in this paper were obtained on the electrodes with diameter 300 μm , which corresponds to an area of $\sim 7 \cdot 10^{-4} \text{ cm}^2$. The size of the electrodes was chosen such that only one capacitor at a time was illuminated by the X-ray focus. We reproducibly reached life times of more than 10^7 switching cycles on different electrodes. We applied a triangular voltage $U(t)$ with different frequencies ν (2-200 kHz), and a peak voltage of $U_{max} = \pm 7 \text{ V}$, which corresponds to an electric field strength of $E = 350 \text{ kV/cm}$, well beyond the coercive field U_c . The triangular voltage was generated using a Keithley 3390 Arbitrary Function Generator. We contacted a single electrode with a tungsten needle with tip diameter 5 μm and used silver paint to contact the bottom electrode in order to apply the field across the PZT layer as described in^{27,28,47}. An Agilent DSO9404A oscilloscope with an input impedance of 50 Ω was used to record the switching current, $I(t)$, and the applied voltage, $U(t)$, across the PZT film during the x-ray diffraction measurement. The polarization was obtained by numerically integrating the measured current $I(t)$ over time. A schematic electrical connection scheme is shown in Figure 1a). Monochromatic X-ray photons with an

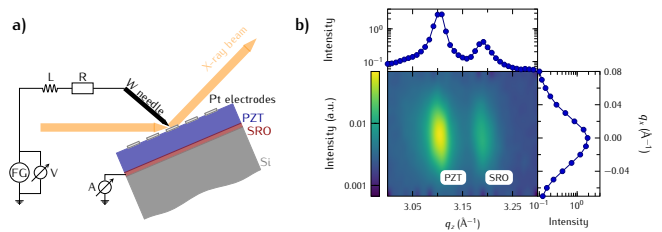


Figure 1. **a)** Schematic electrical circuit of the connected sample (FE) during the measurement and that later is used for the modelling of the response. “FG” denotes the function generator that generates the driving sawtooth voltage, and “osci” represents the two used input channels of the oscilloscope. The voltage amplifier is optional and was only used for low-frequency measurements. **b)** Reciprocal space map of the 002 reflections of PZT and SRO respectively in the pristine state without applied field. The solid symbols are obtained by the integration along the q_x and q_z directions, respectively.

energy of 9 keV were detected by a fast scintillator with a decay time of $\sim 5 \text{ ns}$ combined with a photo multiplier (Hamamatsu H7844). The photo multiplier was read out in single photon counting mode using a time-correlated single photon counter (PicoHarp300, PicoQuant) with an acquisition time window of up to 33 μs ⁴⁷. Asymmetrically scattered X-rays were blocked by a vertical slit of approximately 1 mm width in front of the detector opening. We performed symmetric $\omega/2\theta$ scans with $\omega = \theta$ around the 002 out-of-plane Bragg reflection of PZT. The very good crystalline quality of the PZT and SRO film on Si was characterized by static X-ray diffraction with a Pilatus 100k area detector (Dectris) at the same photon energy. The reconstructed reciprocal space map in Figure 1b) shows the 002 reflections of PZT and SRO, respectively. **The ferroelectric film is oriented with its c-axis out of plane, with negligible x-ray scattering from potential 90° domains.** The time-dependent strain $\eta(t)$ was calculated from the shift of the 002 reflection of PZT along the PZT c -axis as $\eta(t) = (c(t) - c(t=0))/c(t=0)$. All experiments were performed at room temperature.

We first present the frequency-dependent electrical and structural data as $P-U$ and $\eta-U$ hysteresis loops in Figure 2. In Figure 2a) we show the $P-U$ hysteresis loops for frequencies $\nu \leq 20 \text{ kHz}$, which are open saturated loops as expected for a ferroelectric material⁴⁹. **The remanent polarization is rather low, which indicates considerable back switching of domains after saturation. A PUND analysis (not shown) reveals a very small dielectric charging and discharging current with an RC time constant of about 0.1 μs . In addition large switching currents flow for about 25 μs even for each second saturation pulse in the same direction of the PUND sequence. Such slowly responding currents naturally lead to a phase delay of the polarization response which then rounds the hysteresis loop.** As ν is increased from 10 up to $\sim 40 \text{ kHz}$, (Figures 2a) and b) the coercive field U_c increases by almost a factor of 2, consistent with literature results^{50,51}. The double logarithmic plot of U_c versus ν in Figure 2e) repre-

sents a power law $U_c \propto \nu^\beta$ with $\beta = 0.33 = D/6$ over the whole range of ν , which is consistent with a dimensionality $D = 2$ of the domain growth in thin epitaxial films as given by the KAI model^{33,50–54}. The $P - U$ loops at

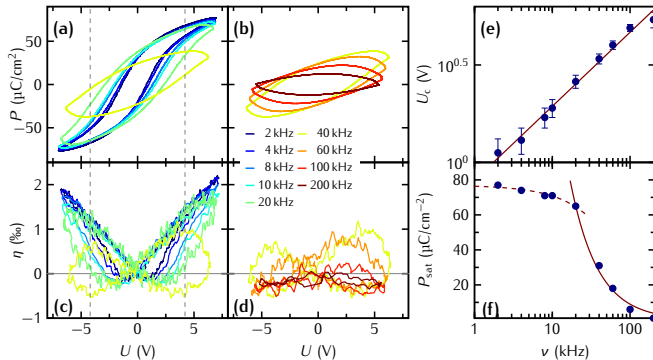


Figure 2. **a-d)** Simultaneously measured $P - U$ and $\eta - U$ loops at different frequencies ν of the applied sawtooth pulse sequence. The panels a) and b) show the $P - U$ loops for $\nu < 40$ kHz and $\nu > 40$ kHz, respectively. In the panels c) and d) we show the corresponding $\eta - U$ loops. In e) we plot U_c (filled circles) from the $P - U$ loops shown in a) and b) on a *double* logarithmic scale as function of ν and the solid line is a fit to the data using ν^β with $\beta = 0.33$. **f)** Plot of the saturation polarization P_{sat} (filled circles) on a *semilogarithmic* scale as function of ν and the dashed line indicates a fit to the data assuming $-\nu$ whereas the solid line indicates a fit using ν^{-1} .

frequencies $\nu \geq 20$ kHz show in contrast rounded shapes and the absence of saturation, which can originate from leakage due to mobile defects like oxygen vacancies in FEs^{51,53,55}. However, such leakage should occur preferentially at low frequency, where the leakage current flows in one direction for a long time and may decrease at high frequency, where also the remanent polarization is smaller because some domains are not switched fast enough⁵⁶. Figures 2c) and d) show that the butterfly loops $\eta - U$ are also simultaneously rounded as the $P(E)$ loops and finally adopt a dumbbell shape where the maximum strain occurs when the driving voltage is already ramped down. This implies that the FE layer is still expanding while the applied voltage is already reduced and that the FE reaches its maximum expansive strain considerably *after* the driving voltage $U(t)$ has reached its maximum value. Simultaneously the saturation polarization P_{sat} is reduced. In Figure 2f), clearly two regimes can be distinguished: For $\nu \leq 20$ kHz, the frequency dependence of P_{sat} follows a $-\nu$ dependence whereas at $\nu \geq 20$ kHz, a polarization is inversely proportional to the frequency ν^{-1} . The frequency at which the cross-over occurs, coincides with the frequency at which the pronounced rounding of the hysteresis loops in Figures 2a-d) is observed.

In the time-domain perspective displayed in Figure 3, the measured polarization $P(t)$ (panel b), which is derived from the current, oscillates in-phase with $U(t)$ (panel a) at low-frequencies. At frequencies $\nu > 40$ kHz,

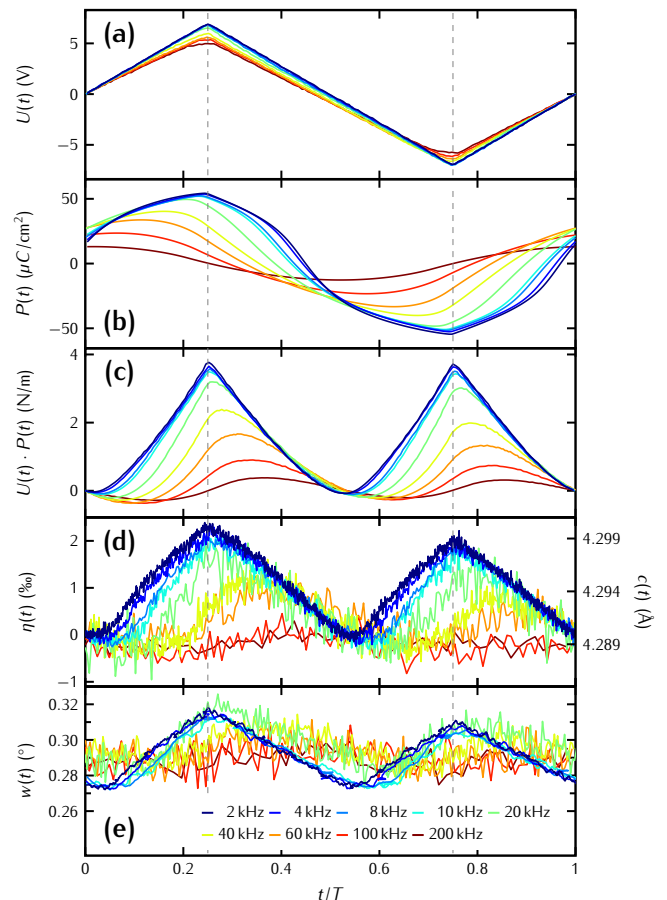


Figure 3. **a)** Applied sawtooth voltage $U(t/T)$ normalized by the period T of the frequency. **b)** Measured polarization $P(t/T)$ of the FE as obtained by the integrator of the switching current over time. **c)** Product $U(t/T) \times P(t/T)$ that closely resembles the time-response of the measured transient strain $\eta(t/T)$ of the FE shown in panel d). **e)** Peak width change $w(t/T)$ of the PZT Bragg reflection.

$P(t)$ is phase-shifted with a value of $\phi_{P-U} = -\pi/2$. This explains the rounded hysteresis loop, because the highest polarization occurs later than the highest voltage. In Figure 3d) we quantify the strain η assuming *via time resolved x-ray diffraction which measures* the absolute values of the c -axis lattice parameter (right vertical axis). We note that at high frequencies the lattice constant reaches smaller values than at any time for low frequency actuation. The lattice is compressed because the polarization and applied voltage are out of phase and hence there are times (e.g. $t/T = 0.25$ to 0.5) where polarization and voltage have opposite sign. This rationalizes the overall negative strain values at high frequency in Figures 2d).

Next we show that the time-dependent piezoelectric stress $\sigma_{\text{FE}} \propto P(t)U(t)$ in Figure 3c) is proportional to the transient polarization $P(t)$ and the applied voltage $U(t)$. The macroscopic polarization $P(t)$ is proportional to the difference in the volume fractions $V_{\text{up}} - V_{\text{down}}$ of the pos-

itively and negatively poled domains, which exhibit the opposite piezoelectric effect. Hence, the piezoelectric coefficient can be approximated by using a time-dependent effective piezoelectric stress coefficient⁵⁷ which we model as $e_{33}(t) = e_{33}^0(2V_{\text{up}}(t)/V - 1) = e_{33}^0(2P_{\text{up}}(t)/P_{\text{sat}} - 1)$, assuming - as a first order approximation neglecting any domain wall contributions - that it is proportional to the volume fractions with up and down polarization, which are in turn described by the averaged polarization. If the entire film of thickness d is poled up we find $e_{33} = e_{33}^0$ in this model and if the entire film is poled down it is $e_{33}(t) = -e_{33}^0$. Thus, the piezoelectric stress

$$\sigma_{\text{FE}} = \frac{e_{33}(t)}{d}U(t) = \frac{e_{33}^0}{d} \left(\frac{2P_{\text{up}}(t)}{P_{\text{sat}}} - 1 \right) U(t) \quad (1)$$

acting on the ferroelectric crystal oscillates at twice the frequency of the driving voltage $U(t)$ because the effective piezoelectric coefficient $e_{33}(t)$ changes its sign together with the voltage, albeit with a phase delay ϕ_{P-U} between $U(t)$ and $P(t)$. We observe that $\phi_{P-U} \leq \pi/2$ for the frequencies investigated in this work. The transient strain $\eta(t)$ (see Figure 3d)) essentially follows the driving stress with the doubled frequency, and exhibits an additional phase shift $\phi_{\sigma-\eta}$ that increases with frequency.

In Figure 3e) we show how the relative peak width $w(t)$ of the PZT 002 Bragg reflection changes for the different applied frequencies. The peak width at high frequencies has a large average value with only small modulation, indicative of a domain pattern with many small domains of up and down polarizations that slightly switch back and forth. At lower frequencies the peak width strongly depends on the currently applied voltage since inhomogeneities of the capacitor dominate the variations of the local expansion.²⁴

In the following we relate the rounding of the hysteresis to the delayed maxima of the $P-U$ loops described by the phase shift ϕ_{P-U} and the characteristic modification of the $\eta-U$ loops to the concomitant stress $\sigma(t)$ to which the strain η responds with an additional phase shift $\phi_{\sigma-\eta}$. To resolve this complex phenomenon of a periodically driven modulation of the FE polarization coupled to the structural deformation we adopt the model describing FE polarization using an oscillator model⁴¹. We set up a system of differential equations for P and η : The voltages at each component in the circuit (see Figure 1a)) add up to the external voltage supplied by the function generator: $U = U_L + U_{\text{FE}} + U_R$. Using the inductance L and resistance R of the circuit including the wiring, the thickness d and dielectric function ϵ_{FE} of the FE capacitor, we can recast this equation in terms of the dielectric displacement $D = \epsilon_0 E + P$ starting from a classical damped harmonic oscillator:

$$L \frac{d^2 D}{dt^2} + R \frac{dD}{dt} + \frac{d}{\epsilon_{\text{FE}}} D = U(t) \quad (2)$$

The strain η within the FE is driven by the same $U(t)$, however, the stress $\sigma_{\text{FE}} = e_{33}(t)U(t)/d \propto P(t)U(t)$ ⁵⁷

couples the differential equation for the strain to Equation 2:

$$\frac{d^2 \eta}{dt^2} + \gamma \frac{d\eta}{dt} + \omega_0^2 \eta = \frac{e_{33}(t)}{d} U(t) \quad (3)$$

where γ is an empirical damping constant and $\omega_0 = 2\pi\nu_0$ is the mechanical angular eigenfrequency of the system. This system of equations challenges theoretical modeling because in the time-dependent perspective, the FE properties are not constant anymore⁴¹. For a full solution the hysteretic behavior of $\epsilon_{\text{FE}}(t)$ must be included, which necessarily adds a memory of the history of the sample. In the following, we use the measured polarization $P(t)$ to rationalize the solution of Equation 3. The time-dependent strain $\eta(t)$ represented in Equation 3 as a damped harmonic oscillator essentially follows the driving stress $\sigma(t)$ at the second harmonic of the driving voltage $U(t)$. The increasing phase delay that η acquires with respect to σ_{FE} allows us to extract a mechanical damping constant that is connected with the viscous properties of the FE domain walls. The lowest mechanical resonance frequency $\nu_0 = 1/T \sim 10$ MHz of the capacitor can be roughly estimated by the time T it takes sound at velocity $v_s \approx 3.5$ nm/ps⁵⁸ to propagate through the diameter $2r = 300$ μm of the electrode $T = 2r/v_s \approx 0.1$ ns. The driving frequency $\nu = 1/T_U \leq 200$ kHz is much lower, as the sawtooth period T_U ranges between 5 and 500 μs . Therefore, we take the textbook result for the phase shift ϕ between $\eta(t)$ and $U(t)$ of the solution to eq. 3 and approximate by

$$\phi_{\eta-U} = \arctan \left(\frac{\gamma\nu}{\nu_0^2 - \nu^2} \right) \approx \arctan \left(\frac{\gamma\nu}{\nu_0^2} \right) \quad (4)$$

Figure 4 shows the excellent agreement of the phase lag determined from the experimental data shown in Figure 3 and the result of Equation 4 with the damping $\gamma = 0.5$ GHz as only fitting parameter. The result is shown by the filled circles in Figure 4 together with the fit to these points using Equation 4 shown as solid line.

In conclusion, this time-domain perspective directly explains how the ferroelectric hysteresis loops in our samples are affected by different driving frequencies: (i) The rounding of the $P-U$ hysteresis is caused by the phase lag between $P(t)$ and $U(t)$, which we relate mainly to the slow domain wall velocity^{24,28}. (ii) For lower frequencies, the polarization can follow the driving voltage, which results in the observed large average stress. (iii) The reduced maximum polarization at high frequencies originates from the fact that at higher frequencies not yet all domains are oriented along the applied field direction when the maximum voltage is reached. This means that at high frequency the coercive field is close to the applied field, however, switching in the same direction continues when the voltage ramps down, as long as a field in the same direction is applied. (iv) The negative average strain of the hysteresis at $\nu = 200$ kHz is a consequence of the phase shifts that let $U(t)$ and $P(t)$, and hence the time-dependent piezoelectric coefficient $d_{33}(t)$

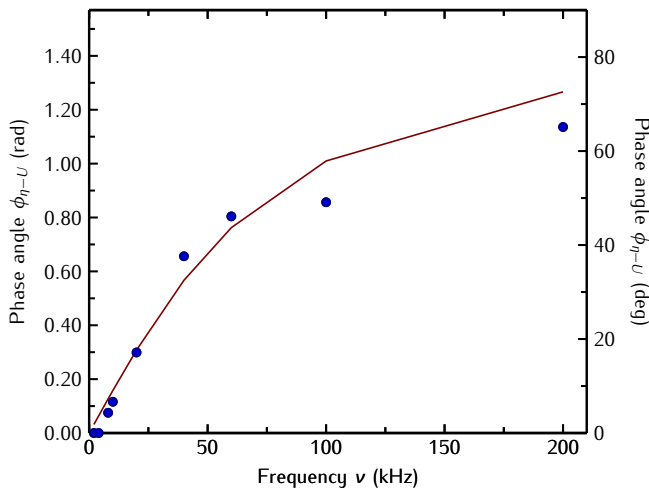


Figure 4. Phase angle $\phi_{\eta-U}$ between the driving voltage $U(t)$ and the strain $\eta(t)$ as function of frequency ν . The filled symbols are extracted from the experimental data and the solid line is the result from the fit using Equation 4 with $\gamma = 0.5$ GHz to the experimental data.

have opposite sign. (v) In part, the increasing coercive field U_c with increasing frequency is a result of the phase lag of the polarization, which implies that the domain wall motion is so slow that the zero crossing of the polarization is only reached later at higher voltage.

We believe that this study is an important contribution to the interpretation of hysteresis loops in the regime of high driving frequencies and hope to stimulate further theoretical and experimental work, that accounts for the complex interplay of polarization and strain via domain-wall motion and viscoelasticity. In the context of application, our study pioneers strain analysis of ferroelectrics integrated on Si with time-resolved x-ray diffraction.

ACKNOWLEDGMENTS

CK, MR, WL and MB acknowledge the BMBF for the financial support via grant No. 05K22IP1. This work was partly realized on the NANOLYON platform. BV, PRR and CD acknowledge the NANOLYON platform and the Agence Nationale de la Recherche (ANR) for support through the grant ANR-14-CE26-0010 (project INTENSE). MB and CD acknowledge the bilateral support of the Deutsche Forschungsgemeinschaft (DFG) and French Agence Nationale de la Recherche (ANR) via the FEAT-project ANR-19-CE24-0027-01, which helped to finalize this manuscript. MR acknowledges fruitful discussions with Thomas Cornelius and Olivier Thomas. MR and MB acknowledge discussions with Thomas Waltinger and Rekikua Alemayehu. MR, MB and CD acknowledge discussions with Dong Jik Kim.

DATA AVAILABILITY STATEMENT

Raw data were generated at the synchrotron storage ring BESSY II operated by Helmholtz-Zentrum Berlin für Materialien und Energie, Germany, large scale facility. Derived data supporting the findings of this study are available from the corresponding authors upon reasonable request.

REFERENCES

- Dawber, M.; Rabe, K. M.; Scott, J. F. Physics of thin-film ferroelectric oxides. *Reviews of Modern Physics* **2005**, *77*, 1083.
- Setter, N.; Damjanovic, D.; Eng, L.; Fox, G.; Gevorgian, S.; Hong, S.; Kingon, A.; Kohlstedt, H.; Park, N. Y.; Stephenson, G. B.; Stolitchnov, I.; Taganstev, A. K.; Taylor, D. V.; Yamada, T.; Streiffer, S. Ferroelectric thin films: Review of materials, properties, and applications. *Journal of Applied Physics* **2006**, *100*, 051606.
- Martin, L. W.; Rappe, A. M. Thin-film ferroelectric materials and their applications. *Nature Reviews Materials* **2017**, *2*, 16087.
- Gregg, J. M. Ferroelectrics at the nanoscale. *physica status solidi (a)* **2009**, *206*, 577–587.
- Fridkin, V. M.; Ducharme, S. Ferroelectricity at the nanoscale. *Uspekhi Fizicheskikh Nauk* **2014**, *184*, 645–651.
- Yang, S. M.; Morozovska, A. N.; Kumar, R.; Eliseev, E. A.; Cao, Y.; Mazet, L.; Balke, N.; Jesse, S.; Vasudevan, R. K.; Dubourdieu, C.; Kalinin, S. V. Mixed electrochemical-ferroelectric states in nanoscale ferroelectrics. *Nature Physics* **2017**, *13*, 812–818.
- McKee, R. A.; Walker, F. J.; Chisholm, M. F. Crystalline Oxides on Silicon: The First Five Monolayers. *Physical Review Letters* **1998**, *81*, 3014–3017.
- Vaithyanathan, V.; Lettieri, J.; Tian, W.; Sharan, A.; Vasudevarao, A.; Li, Y. L.; Kochhar, A.; Ma, H.; Levy, J.; Zschack, P.; Woicik, J. C.; Chen, L. Q.; Gopalan, V.; Schlom, D. G. *c*-axis oriented epitaxial BaTiO₃ films on (001) Si. *Journal of Applied Physics* **2006**, *100*, 024108.
- Reiner, J. W.; Kolpak, A. M.; Segal, Y.; Garrity, K. F.; Ismail-Beigi, S.; Ahn, C. H.; Walker, F. J. Crystalline Oxides on Silicon. *Advanced Materials* **2010**, *22*, 2919–2938.
- Baek, S. H. et al. Giant Piezoelectricity on Si for Hyperactive MEMS. *Science* **2011**, *334*, 958–961.
- Mazet, L.; Yang, S. M.; Kalinin, S. V.; Schamm-Chardon, S.; Dubourdieu, C. A review of molecular beam epitaxy of ferroelectric BaTiO₃/subfilms on Si, Ge and GaAs substrates and their applications. *Science and Technology of Advanced Materials* **2015**, *16*, 036005.
- Louahadj, L.; Bourdais, D. L.; Largeau, L.; Agnus, G.; Mazet, L.; Bachelet, R.; Regreny, P.; Albertini, D.; Pillard, V.; Dubourdieu, C.; Gautier, B.; Lecoeur, P.; Saint-Girons, G. Ferroelectric Pb(Zr,Ti)O₃/sub epitaxial layers on GaAs. *Applied Physics Letters* **2013**, *103*, 212901.
- Trolier-McKinstry, S.; Zhang, S.; Bell, A. J.; Tan, X. High-Performance Piezoelectric Crystals, Ceramics, and Films. *Annual Review of Materials Research* **2018**, *48*, 191–217.
- Noheda, B.; Cox, D. E.; Shirane, G.; Gonzalo, J. A.; Cross, L. E.; Park, S.-E. A monoclinic ferroelectric phase in the Pb(Zr_{1-x}Ti_x)O₃ solid solution. *Applied Physics Letters* **1999**, *74*, 2059–2061.
- Noheda, B.; Gonzalo, J. A.; Cross, L. E.; Guo, R.; Park, S.-E.; Cox, D. E.; Shirane, G. Tetragonal-to-monoclinic phase transition in a ferroelectric perovskite: The structure of PbZr_{0.52}Ti_{0.48}O₃. *Physical Review B* **2000**, *61*, 8687–8695.
- Noheda, B.; Cox, D. E.; Shirane, G.; Guo, R.; Jones, B.; Cross, L. E. Stability of the monoclinic phase in the ferroelectric perovskite. *Physical Review B* **2000**, *63*, 014103.

- ¹⁷Zhang, N.; Yokota, H.; Glazer, A. M.; Ren, Z.; Keen, D. A.; Keeble, D. S.; Thomas, P. A.; Ye, Z.-G. The missing boundary in the phase diagram of $\text{PbZr}_{1-x}\text{Ti}_x\text{O}_3$. *Nature Communications* **2014**, *5*, 5231.
- ¹⁸Kim, D. M.; Eom, C. B.; Nagarajan, V.; Ouyang, J.; Ramesh, R.; Vaithyanathan, V.; Schlom, D. G. Thickness dependence of structural and piezoelectric properties of epitaxial $\text{Pb}(\text{Zr}_{0.52}\text{Ti}_{0.48})\text{O}_3$ films on Si and SrTiO_3 substrates. *Applied Physics Letters* **2006**, *88*, 142904.
- ¹⁹Dekkers, M.; Nguyen, M. D.; Steenwelle, R.; te Riele, P. M.; Blank, D. H. A.; Rijnders, G. Ferroelectric properties of epitaxial $\text{Pb}(\text{Zr},\text{Ti})\text{O}_3$ thin films on silicon by control of crystal orientation. *Applied Physics Letters* **2009**, *95*, 012902.
- ²⁰Sambri, A.; Gariglio, S.; Pardo, A. T.; Triscone, J.-M.; Stéphan, O.; Reiner, J. W.; Ahn, C. H. Enhanced critical temperature in epitaxial ferroelectric $\text{Pb}(\text{Zr}_{0.2}\text{Ti}_{0.8})\text{O}_3$ thin films on silicon. *Applied Physics Letters* **2011**, *98*, 012903.
- ²¹Chirila, C.; Boni, A. G.; Pasuk, I.; Negrea, R.; Trupina, L.; Rhun, G. L.; Yin, S.; Vilquin, B.; Pintilie, I.; Pintilie, L. Comparison between the ferroelectric/electric properties of the $\text{PbZr}_{0.52}\text{Ti}_{0.48}\text{O}_3$ films grown on Si (100) and on STO (100) substrates. *Journal of Materials Science* **2015**, *50*, 3883–3894.
- ²²v. Korff Schmising, C.; Bargheer, M.; Kiel, M.; Zhavoronkov, N.; Woerner, M.; Elsaesser, T.; Vrejoiu, I.; Hesse, D.; Alexe, M. Coupled Ultrafast Lattice and Polarization Dynamics in Ferroelectric Nanolayers. *Physical Review Letters* **2007**, *98*, 257601.
- ²³Mankowsky, R.; von Hoegen, A.; Först, M.; Cavalleri, A. Ultrafast Reversal of the Ferroelectric Polarization. *Physical Review Letters* **2017**, *118*, 197601.
- ²⁴Grigoriev, A.; Do, D.-H.; Kim, D. M.; Eom, C.-B.; Adams, B.; Dufresne, E. M.; Evans, P. G. Nanosecond Domain Wall Dynamics in Ferroelectric Thin Films. *Physical Review Letters* **2006**, *96*, 187601.
- ²⁵Jo, J. Y.; Chen, P.; Sichel, R. J.; Callori, S. J.; Sinsheimer, J.; Dufresne, E. M.; Dawber, M.; Evans, P. G. Nanosecond Dynamics of Ferroelectric/Dielectric Superlattices. *Physical Review Letters* **2011**, *107*, 055501.
- ²⁶Zhang, Q.; Herchig, R.; Ponomareva, I. Nanodynamics of Ferroelectric Ultrathin Films. *Physical Review Letters* **2011**, *107*, 177601.
- ²⁷Kwamen, C.; Rössle, M.; Reinhardt, M.; Leitenberger, W.; Zamponi, F.; Alexe, M.; Bargheer, M. Simultaneous dynamic characterization of charge and structural motion during ferroelectric switching. *Physical Review B* **2017**, *96*, 134105.
- ²⁸Kwamen, C.; Rössle, M.; Leitenberger, W.; Alexe, M.; Bargheer, M. Time-resolved X-ray diffraction study of the structural dynamics in an epitaxial ferroelectric thin $\text{Pb}(\text{Zr}_{\text{sub}0.2/\text{sub}0.8}\text{Ti}_{\text{sub}0.8/\text{sub}0.2})\text{O}_3$ film induced by sub-coercive fields. *Applied Physics Letters* **2019**, *114*, 162907.
- ²⁹Akamatsu, H.; Yuan, Y.; Stoica, V. A.; Stone, G.; Yang, T.; Hong, Z.; Lei, S.; Zhu, Y.; Haislmaier, R. C.; Freeland, J. W.; Chen, L.-Q.; Wen, H.; Gopalan, V. Light-Activated Gigahertz Ferroelectric Domain Dynamics. *Physical Review Letters* **2018**, *120*, 096101.
- ³⁰Kolmogorov, A. N. Statistical theory of metal crystallization. *Izv. Akad. Nauk SSSR, Ser. Mat.* **1937**, *3*, 355–359.
- ³¹Avrami, M. Kinetics of Phase Change. II Transformation-Time Relations for Random Distribution of Nuclei. *The Journal of Chemical Physics* **1940**, *8*, 212–224.
- ³²Ishibashi, Y. A Model of Polarization Reversal in Ferroelectrics. *Journal of the Physical Society of Japan* **1990**, *59*, 4148–4154.
- ³³Orihara, H.; Hashimoto, S.; Ishibashi, Y. A Theory of D-E Hysteresis Loop Based on the Avrami Model. *Journal of the Physical Society of Japan* **1994**, *63*, 1031–1035.
- ³⁴Lee, K. S.; Kim, Y. K.; Baik, S.; Kim, J.; Jung, I. S. In situ observation of ferroelectric 90° -domain switching in epitaxial $\text{Pb}(\text{Zr},\text{Ti})\text{O}_3$ thin films by synchrotron x-ray diffraction. *Applied Physics Letters* **2001**, *79*, 2444–2446.
- ³⁵Wallace, M.; Johnson-Wilke, R. L.; Esteves, G.; Fancher, C. M.; Wilke, R. H. T.; Jones, J. L.; Trolier-McKinstry, S. In situ measurement of increased ferroelectric/ferroelastic domain wall motion in de-clamped tetragonal lead zirconate titanate thin films. *Journal of Applied Physics* **2015**, *117*, 054103.
- ³⁶Davydok, A.; Cornelius, T.; Mocuta, C.; Lima, E.; Araujo, E.; Thomas, O. In situ X-ray diffraction studies on the piezoelectric response of PZT thin films. *Thin Solid Films* **2016**, *603*, 29–33.
- ³⁷Nagarajan, V.; Jenkins, I. G.; Alpay, S. P.; Li, H.; Aggarwal, S.; Salamanca-Riba, L.; Roytburd, A. L.; Ramesh, R. Thickness dependence of structural and electrical properties in epitaxial lead zirconate titanate films. *Journal of Applied Physics* **1999**, *86*, 595–602.
- ³⁸Gariglio, S.; Stucki, N.; Triscone, J.-M.; Triscone, G. Strain relaxation and critical temperature in epitaxial ferroelectric $\text{Pb}(\text{Zr}_{0.20}\text{Ti}_{0.80})\text{O}_3$ thin films. *Applied Physics Letters* **2007**, *90*, 202905.
- ³⁹Ryding, S.; Cernik, R.; Wooldridge, J.; Burnett, T.; Stewart, M.; Vecchini, C.; Cain, M.; Lennie, A.; Yuan, F.; Tang, C.; Thompson, P. Simultaneous measurement of X-ray powder diffraction and ferroelectric polarisation data as a function of applied electric field at a range of frequencies. *Powder Diffraction* **2013**, *18*, S220.
- ⁴⁰Wooldridge, J.; Ryding, S.; Brown, S.; Burnett, T. L.; Cain, M. G.; Cernik, R.; Hino, R.; Stewart, M.; Thompson, P. Simultaneous measurement of X-ray diffraction and ferroelectric polarization data as a function of applied electric field and frequency. *Journal of Synchrotron Radiation* **2012**, *19*, 710–716.
- ⁴¹Barz, K.; Diestelhorst, M.; Beige, H. Amplitude Frequency Characteristics of Ferroelectric Thin Film Structures. *Ferroelectrics* **2010**, *396*, 27–36.
- ⁴²Mazet, L.; Bachelet, R.; Louahadj, L.; Albertini, D.; Gautier, B.; Cours, R.; Schamm-Chardon, S.; Saint-Girons, G.; Dubourdieu, C. Structural study and ferroelectricity of epitaxial $\text{BaTiO}_3/\text{sub}$ films on silicon grown by molecular beam epitaxy. *Journal of Applied Physics* **2014**, *116*, 214102.
- ⁴³Borowiak, A.; Niu, G.; Pillard, V.; Agnus, G.; Lecoeur, P.; Albertini, D.; Baboux, N.; Gautier, B.; Vilquin, B. Pulsed laser deposition of epitaxial ferroelectric $\text{Pb}(\text{Zr},\text{Ti})\text{O}_3$ films on silicon substrates. *Thin Solid Films* **2012**, *520*, 4604–4607.
- ⁴⁴Yin, S.; Niu, G.; Vilquin, B.; Gautier, B.; Rhun, G. L.; Defay, E.; Robach, Y. Epitaxial growth and electrical measurement of single crystalline $\text{Pb}(\text{Zr}_{0.52}\text{Ti}_{0.48})\text{O}_3$ thin film on Si(001) for micro-electromechanical systems. *Thin Solid Films* **2012**, *520*, 4572–4575.
- ⁴⁵Boni, A. G.; Chirila, C.; Pasuk, I.; Negrea, R.; Trupina, L.; Rhun, G. L.; Vilquin, B.; Pintilie, I.; Pintilie, L. Electrode interface controlled electrical properties in epitaxial $\text{Pb}(\text{Zr}_{0.52}\text{Ti}_{0.48})\text{O}_3$ films grown on Si substrates with SrTiO_3 buffer layer. *Thin Solid Films* **2015**, *593*, 124–130.
- ⁴⁶Bouregba, R.; Poullain, G.; Vilquin, B.; Rhun, G. L. Asymmetrical leakage currents as a possible origin of the polarization offsets observed in compositionally graded ferroelectric films. *Journal of Applied Physics* **2003**, *93*, 5583–5591.
- ⁴⁷Rössle, M.; Leitenberger, W.; Reinhardt, M.; Koç, A.; Pudell, J.; Kwamen, C.; Bargheer, M. The time-resolved hard X-ray diffraction endstation KMC-3 XPP at BESSY II. *Journal of Synchrotron Radiation* **2021**, *28*, 948–960.
- ⁴⁸Holladack, K.; Ovsyannikov, R.; Kuske, P.; Müller, R.; Schällicke, A.; Scheer, M.; Gorgoi, M.; Kühn, D.; Leitner, T.; Svensson, S.; Mårtensson, N.; Föhlisch, A. Single bunch X-ray pulses on demand from a multi-bunch synchrotron radiation source. *Nature Communications* **2014**, *5*, 4010.
- ⁴⁹Scott, J. F. Ferroelectrics go bananas. *Journal of Physics: Condensed Matter* **2008**, *20*, 021001.
- ⁵⁰Mukhortov, V., V.M. and Kolesnikov; Biryukov, S.; Golovko, Y.; Maschenko, A. Dynamics of polarization reversal in thin PZT films. **2005**,
- ⁵¹Yang, S. M.; Jo, J. Y.; Kim, T. H.; Yoon, J.-G.; Song, T. K.; Lee, H. N.; Marton, Z.; Park, S.; Jo, Y.; Noh, T. W. ac dynamics of ferroelectric domains from an investigation of the frequency dependence of hysteresis loops. *Physical Review B* **2010**,

82, 174125.

- ⁵²Ishibashi, Y.; Orihara, H. A theory of D-E hysteresis loop. *Integrated Ferroelectrics* **1995**, *9*, 57–61.
- ⁵³Scott, J. F. Models for the frequency dependence of coercive field and the size dependence of remanent polarization in ferroelectric thin films. *Integrated Ferroelectrics* **1996**, *12*, 71–81.
- ⁵⁴Li, W.; Chen, Z.; Auciello, O. Calculation of frequency-dependent coercive field based on the investigation of intrinsic switching kinetics of strained $\text{Pb}(\text{Zr}_{0.2}/\text{Ti}_{0.8})\text{O}_3$ thin films. *Journal of Physics D: Applied Physics* **2011**, *44*, 105404.

- ⁵⁵Liu, Y.-T.; Chiu, S.-J.; Lee, H.-Y.; Chen, S.-Y. Fabrication and ferroelectric properties of $\text{BiFeO}_3/\text{LaNiO}_3$ artificial superlattice structures grown by radio-frequency magnetron-sputtering. *Thin Solid Films* **2013**, *529*, 66–70.
- ⁵⁶Hashimoto, S.; Orihara, H.; Ishibashi, Y. Study on D/E-Hysteresis Loop of TGS Based on the Avrami-Type Model. *Journal of the Physical Society of Japan* **1994**, *63*, 1601–1610.
- ⁵⁷Trolier-McKinstry, S.; Gharb, N. B.; Damjanovic, D. Piezoelectric nonlinearity due to motion of 180° domain walls in ferroelectric materials at subcoercive fields: A dynamic poling model. *Applied Physics Letters* **2006**, *88*, 202901.
- ⁵⁸Tawfik, A. Communications of the American Ceramic Society. *Journal of the American Ceramic Society* **1985**, *68*, C-317–C-319.